Impact of social distancing on disease transmission risk in the context of a pandemic

Chuan-Yao Li,[1] Jie Yin,[1] and Liang Chen[2,*]

[1]*School of Traffic and Transportation Engineering, Central South University, Changsha 410075, China*

[2]*Beijing Key Laboratory of Traffic Engineering, Beijing University of Technology, Beijing 100124, China*

(Received 28 June 2023; revised 28 September 2023; accepted 12 October 2023; published 9 November 2023)

Changes in pedestrian dynamics caused by social distancing policies place new demands on pedestrian motion modeling during the pandemic. This study summarizes pedestrian movement characteristics during the pandemic, based on which, the traditional floor-field cellular automata model was improved by introducing two floor fields related to pedestrian density to simulate social distancing in crowded places. Especially, the cumulative density field guides pedestrians in route selection, thereby compensating for the limitation of the previous models in which only local repulsion was considered. By selecting an appropriate combination of parameters, the desired social distancing behavior can be observed. Then, the rationality of our model is verified by the fundamental diagram. Moreover, to assess the influences of social distancing on the risk of disease transmission, we considered both person-person transmission and environment-person transmission. The simulation results show that although social distancing is effective in preventing interpersonal transmission, an increase in environmental transmission may somewhat offset this effect. We also examined the influence of individual motion heterogeneity on infection spread and found that the containment was the best when only patients complied with the social distancing restriction. The trade-off between safety and efficiency associated with social distancing was also initially explored in this study.

DOI: 10.1103/PhysRevE.108.054115

I. INTRODUCTION

Humans have been fighting infectious diseases since the Athens plague in 430 BC [1]. The emergence of smallpox, plague, as well as COVID-19 pneumonia, and other infectious diseases, not only directly caused animal or human casualties, but also caused a series of problems, such as social panic, economic recession, and so on. With the development of science and technology, mankind has also developed various methods for combating unpredictable infectious diseases [2–4]. Social distancing (hereinafter referred to as SD) is one of the most common nonpharmacological interventions, which refers to the establishment of a physical barrier between two or more persons to suppress the spread of the virus [5]. The experiences of Philadelphia and St. Louis are often compared to demonstrate how SD interventions worked in preventing disease transmission [6]. During the Spanish flu pandemic, St. Louis established strict SD measures early on, while Philadelphia implemented minimal restrictions much later. As a result, the outbreak in St. Louis was milder, while Philadelphia had one of the highest death rates in the United States. It is therefore essential to apply SD restrictions to populations for infectious diseases for which no effective vaccine has been developed. Similarly, the desire for SD during the COVID-19 epidemic became a key concept in media coverage on how to stop the disease from spreading further [7,8].

Social distancing can be implemented centrally, such as by closing schools and workplaces and canceling activities, or it can occur naturally as a result of individual actions. Some studies have used macromodeling methods to explore the effect of large-scale and centralized SD policies on epidemic prevention and control. Milne *et al.* modeled pandemic influenza transmission within a small community based on household demographics, intracommunity mobility, and individual interaction patterns [9]. The effects of four kinds of SD interventions were then evaluated: school closures, case isolation, work absences, and community lockdowns. Early and sustained multiple SD measures were detected to be helpful in containing a pandemic. Epstein *et al.* used an equation-based epidemiological model to explore the influence of reducing air travel on the global propagation of infectious diseases [10]. The results suggest that restrictions on international air travel may slightly slow the spread of the epidemic across regions. Supporting evidence is presented by Brownstein *et al.* that the grounding of U.S. flights after September 11, 2001 delayed the flu dynamics for the 2001–2002 season by about two weeks [11]. In addition, isolation policies have been shown to be a good tool for disease attenuation, especially in endemic areas with relatively high disease progression rates [12,13]. As for SD at the level of individual actions, different countries and organizations put forward various distance restrictions. For instance, when the COVID-19 epidemic broke out in 2020, the World Health Organization recommended a physical distancing of 1 m or more when performing public activities. Accordingly, the United States, the United Kingdom, and Canada have adopted distancing policies of 6 feet and 2 m in public spaces, respectively. During a pandemic, maintaining SD inevitably becomes the new normal of human life, leading to drastic changes in pedestrian dynamics in public spaces.

*Corresponding author: liangchen@bjut.edu.cn

Thus, it is essential for researchers to understand and quantify this shift.

Studies have begun to look at shifts in real population dynamics in the pandemic environment through experiments, field observations, social distancing detection, and monitoring algorithms. At present, several researchers have carried out a series of new pedestrian movement experiments, exploring the speed-density and headway-speed relation in pedestrian flow with physical distancing requirements and determining the limit of crowd density that can guarantee a SD of 1 m [14–16]. Tanis *et al.* collected a series of SD motion datasets from experiments with different walking directions and behavioral interventions [17]. Hayes *et al.* obtained the movement characteristics of passengers getting on and off the train when the SD policy was adopted by analyzing CCTV footage taken at the railway platform [18]. Similarly, the comparison of videos of a railway station before and during the pandemic was made by Pouw *et al.* [19]. They also used sparse graphs to estimate the physical distancing and exposure time of pedestrians. In the specific field of pedestrian detection and monitoring algorithms, epidemic-related research focuses on the issue of visual SD, which means using cameras and other imaging sensors to automatically estimate distances between individuals in real time [20,21]. Visual SD provides a noninvasive way to determine if individuals in a crowd maintain safe physical distances, thereby identifying potential hotspots for distancing violations.

From the above studies, we can learn that real crowd dynamics have undergone great changes due to SD policies. To study adaptive traffic planning in time for restoring more pedestrian mobility in public spaces, there is an urgent need to address the shift in pedestrian behavior from a normal to an epidemic state in simulations. At present, some researchers have introduced SD into pedestrian simulation systems. For example, the traditional social force model has been revised to take into account the psychological factors and avoidance behavior of pedestrian movement during the epidemic. Researchers modified the algorithm of the pedestrian driving force and repulsion interaction force, or the desired distance pedestrians want to maintain, and then simulated SD scenarios using a combination of parameter calibration and operational improvement [22–25]. Silva *et al.* constructed a new agent-based model to analyze the impact of seven SD measures on pandemic dynamics [26]. Trying to simulate SD, Mayr and Köster updated the optimal steps model in the pedestrian simulator VADERE [27]. Two parameters in the model were systematically studied to find the combination of parameters that is best suited to observe imposed SD behavior in crowds. Parisi *et al.* simulated pedestrian movement in a supermarket using an agent-based model [28]. The number and duration of events with a physical distance of less than 2 m in the simulation system were calculated to explore how the number of pedestrians affected safe distances.

Available evidence suggests that the main trend in microsocial distancing modeling remains to resort to straightforward mechanisms of repulsion or avoidance, such as the repulsive force in social force models. However, since not all pedestrian simulation models contain a core of motion layer which is based on social forces, further research is needed to determine how to control the distance between agents in the absence of a non–social-force framework. When discussing the challenges and opportunities of crowd modeling in the pandemic era, Haghani also emphasized the need to further investigate whether grid-based models can use more direct parameter changes to make agents avoid cells that are in close proximity to another agent [29]. To the best of our knowledge, no cellular automata have been used for SD simulation.

In addition, pedestrian dynamics is fused with epidemiology to study microscopic infection spread on an individual scale. These studies tend to focus on crowded scenarios, such as foot traffic at train stations [30], daily activities on cruise ships [31], airline boarding and alighting policies [32–34], pedestrian movements on college campuses [35], as well as shopping malls [36]. These studies considered people's movements when maintaining traditional human distancing. However, in these cases, the influence of physical distancing between pedestrians on the dynamics of disease transmission has received little attention. Population-level SD measures, such as closing schools, canceling mass gatherings, and quarantining cases, have proven to be effective in containing epidemics. The impact of SD at the individual level on disease transmission remains to be further explored [37].

To fill the above research gaps, this study will design a grid-based pedestrian social distancing model by introducing pedestrians' antiepidemic psychology. We introduce two floor fields related to crowd density to describe the pedestrian's spontaneous decision-making behavior and group phenomenon under the SD policy. The local density field is used to describe the local repulsion of pedestrians. The cumulative density field represents the global route information and helps pedestrians choose routes with less congestion, which cannot be achieved by the above social force model and agent-based model that only considers local repulsion. Previously, global route information was commonly used for shortest route planning, but it has not been used for pedestrian evacuation simulation in the context of a pandemic. Therefore, we hope to overcome the limitations of models that only consider local repulsion and incorporate global density information in cellular automata (CA), allowing a more detailed analysis of the role of pedestrian microscopic risk-avoiding behavior in containing disease transmission. Moreover, different modes of disease transmission are considered in this paper for better application extensibility.

The remainder of this paper is organized as follows. We modify the traditional floor-field cellular automata model to depict individuals' spontaneous SD behavior in Sec. II In Sec. III, the key parameters significantly affecting pedestrians' SD behavior are identified through a combination of visual observation and sensitivity analysis. Then, we validate our model using the fundamental diagram in Sec. IV. In Section 5, we evaluate the influence of SD on the risk of disease transmission through numerical experiments. The conclusions of our study are summarized and future research prospects are presented in Sec. VI.

II. MODEL FORMULATION

Our work aims to study the spontaneous SD behavior of individuals. An individual's decision can be influenced by many factors, including infection awareness, government

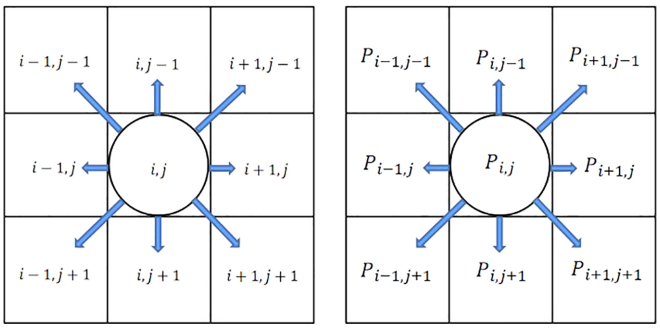

FIG. 1. Sketch of Moore neighborhood. Pedestrian at cell (i, j) can move to its eight neighboring cells or be immobile in original cell at each time step.

advice, and psychological factors. Through an extensive collection of relevant social psychology literature [38,39], video observations [18,19], real pedestrian experiments [14–17], online questionnaires [40–42], etc., we can summarize the characteristics of pedestrian movement during the pandemic: (1) Pedestrians have a tendency to keep greater physical distances from the crowd around them, and the space required for walking increases. (2) When choosing a route, most pedestrians tend to move towards areas with fewer pedestrians to avoid crowd gathering. (3) Pedestrians are more purposeful when moving, which means their walking direction is more monotonous and will not be easily changed. These observations encouraged us to build a motion model to simulate pedestrian evacuation during a pandemic.

As a typical pedestrian and evacuation dynamic model, the floor-field cellular automata (FFCA) model has unique advantages in terms of scalability, such as representation of individual attributes, faster computation, and so on. The FFCA model is designed to reproduce herding behavior and shortest path-finding behavior during evacuation [43], applicable to incorporating other social and psychological factors in pedestrian movement simulations due to its flexibility and scalability [44,45]. However, the general FFCA model has not been extended to the simulation of SD behavior in crowd evacuation and is not suitable for pedestrian movement simulation in the context of a pandemic. Therefore, based on the traditional FFCA model, this study improved the expression of pedestrian movement choice by considering the psychological factors of pedestrians, namely the instinct to avoid others and move towards low pedestrian-density areas during a pandemic.

First, the whole space is divided into a two-dimensional grid of square cells, where each cell occupies an area of $0.25\,\mathrm{m}^2$ [46]. The pedestrian movement of each time step is updated by using the Moore neighborhood, as shown in Fig. 1. The pedestrian at cell (i, j) can move to its eight neighboring cells or be immobile in the original cell at each time step. The transfer probability depends entirely on the potentials of these nine cells in the Moore neighborhood, defined as follows:

$$P_{i,j}^{x,y} = \frac{N_{x,y}}{\sum_{m=i-1}^{i+1}\sum_{n=j-1}^{j+1} N_{m,n}}$$
$$x \in [i-1, i+1]\,;\; y \in [j-1, j+1], \qquad (1)$$

where $P_{i,j}^{x,y}$ refers to the probability of pedestrian at cell (i, j) moving to cell (x, y), and $N_{x,y}$ refers to the potential of cell (x, y). This is a normalization method where all nine transfer probabilities add up to a value of 1. $N_{x,y}$ is relevant to four floor fields, that is,

$$N_{x,y} = E_{x,y}\exp(k_s S_{x,y} + k_O O_{x,y} + k_L L_{x,y} + k_C C_{x,y}), \qquad (2)$$

where $E_{x,y}$ is a 0–1 variable indicating if cell (x, y) is in the occupation of a pedestrian or an obstacle. If cell (x, y) is empty, the value of $E_{x,y}$ is 1; otherwise, it is 0.

The four floor fields used to describe the different movement characteristics of pedestrians are defined as follows:

Finding the shortest path: $S_{x,y}$ represents the Euclidean distance from cell (x, y) to the destination, calculated as follows:

$$S_{x,y} = \min\{\sqrt{(x-x_0)^2 + (y-y_0)^2}\,|(x_0, y_0) \in \phi,\ \phi \text{ is the set of exits}\}. \qquad (3)$$

Obstacle avoidance: $O_{x,y}$ denotes the repulsion of obstacles to pedestrian movement, with a value of the number of nonobstacle cells in the eight adjacent cells of cell (x, y).

Pedestrian repulsion: $L_{x,y}$ represents the local density of people around cell (x, y) and is used to describe the instinct of pedestrians to avoid surrounding pedestrians. Its value is the number of pedestrians within the Moore neighborhood of the cell (x, y).

Moving towards low-density region: $C_{x,y}$ represents the cumulative density of the route from cell (x, y) to the destination, that is, the accumulation of pedestrian density in each cell that the route passes through. It is used to describe the tendency of pedestrians to move towards areas with fewer pedestrians. The greater $C_{x,y}$, the more pedestrians may be encountered on the route, and the smaller the possibility of moving towards cell (x, y). It is calculated as follows $[C_{x,y} = C(x, y)]$:

$$C(x,y) = \int_{x,y}^{x_0,y_0} g(x,y)ds = \int_{x,y}^{x_0,y_0} (g(x,y)x'(s)dx + g(x,y)y'(s)dy), \qquad (4)$$

where $g(x, y)$ gives the density distribution of pedestrians in cell space. The average pedestrian density of 25 cells in a square centered on cell (x, y) is calculated as the density of cell (x, y) [47]. The integration path is represented by $l : x = x(s), y = y(s)$, and $ds = \sqrt{dx^2 + dy^2}$. The unit vector $[x'(s), y'(s)]$ points to the direction of integration. To guarantee that $C(x, y)$ is a single-valued function, we must assume that the integral is path independent, namely:

$$C_x(x,y) = -g(x,y)x'(s)\ ,\ C_y(x,y) = -g(x,y)y'(s). \qquad (5)$$

Equation (5) leads to the following Eikonal equation:

$$\sqrt{C_x^2(x,y) + C_y^2(x,y)} = g(x,y). \qquad (6)$$

By setting $C(x_0, y_0) = 0$ as the boundary condition, $C(x, y)$ in the Eikonal equation (6) can be solved numerically by the fast-sweeping method [48].

In the improved FFCA model, $S_{x,y}$ and $O_{i,j}$ form a static floor field, which describes the behavior of pedestrians searching for the shortest route to their destination, and also reflects the distribution of obstacles, while $L_{x,y}$ and $C_{x,y}$ constitute a dynamic floor field, which describes pedestrians' antiepidemic psychology to avoid close contact with others. The static floor field does not change with the simulation time step, while the dynamic floor field needs to be updated at each time step due to the change of pedestrian position.

In Eq. (2), k_S, k_O, k_L, and k_C are corresponding parameters. $N_{x,y}$ drops with $S_{x,y}$ and $L_{x,y}$, and $C_{x,y}$,increases with $O_{i,j}$, so $k_S < 0$, $k_L < 0$, $k_C < 0$, $k_O > 0$.

III. PARAMETER SETTING

This section tries to assess the influence of different floor fields in the model established above on pedestrians' behaviors, adopting a combination of visual observation and sensitivity analysis. The parameters that have significant impacts on crowd movement and their range of values are determined. To examine the extent to which pedestrians' spontaneous risk-avoiding behavior promotes the formation of SD, and to lay the foundation for subsequent simulation experiments, we will identify the combination of parameters that yields the optimal SD effect.

The constructed model is used in the simulation of crowd evacuation in a simplified four-exit room. The room covers an area of a 100×100 grid with four 12-grid-wide exits and randomly distributed obstacles inside. The total number of pedestrians is 500, randomly and evenly distributed in the room at the beginning. Since our study focuses primarily on reproducing pedestrians' SD behavior, we fix the coefficients $k_S = -5$ and $k_O = 2$, and observe the impact of local density and cumulative density on pedestrian motion by systematically varying the values of k_L and k_C. For each parameter combination, the simulation is run 50 times. We want pedestrians to maintain a physical distance of 1 m in the simulation, corresponding to the safe interpersonal distance for many respiratory infectious diseases.

A. Visual observation

First, we set the following four parameter combinations for simulation: (a) $k_L = 0$, $k_C = 0$, which represents that neither local density nor cumulative density is considered during pedestrian evacuation; (b) $k_L = -20$, $k_C = 0$, which represents that only local density is considered; (c) $k_L = 0$, $k_C = -20$, which represents that only cumulative density is considered; and (d) $k_L = -20$, $k_C = -20$, which represents that both local density and cumulative density are considered. Using the simulation data for each time step, the crowd movement at different moments during the evacuation can be graphically displayed. Figure 2 presents the spatial distribution of crowd in different simulation experiments when 200 pedestrians have left and only 300 pedestrians remain in the room. Comparing Fig. 2(a) with Fig. 2(d), we can see that by introducing two floor fields related to pedestrian density, SD behavior can be reproduced among pedestrians. And, local density is more likely to trigger SD between pedestrians [comparing Fig. 2(b) with Fig. 2(c)], which is consistent with previous theories.

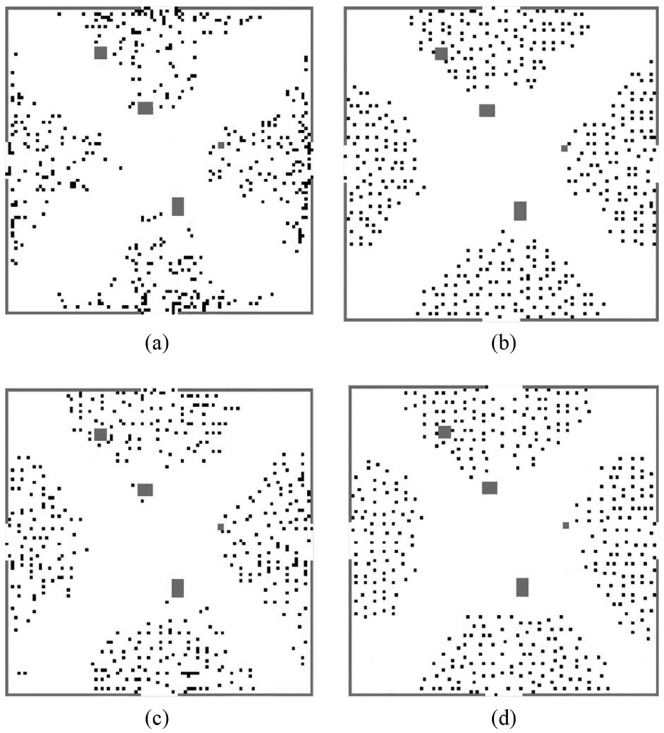

FIG. 2. Screenshots of evacuation process when k_L and k_C take different values: (a) $k_L = 0$, $k_C = 0$; (b) $k_L = -20$, $k_C = 0$; (c) $k_L = 0$, $k_C = -20$; and (d) $k_L = -20$, $k_C = -20$. Screenshot moment is when 200 pedestrians have left and only 300 pedestrians remain in room. Black dots represent pedestrians and gray squares represent obstacles.

As shown in Fig. 2, an arch-shaped crowd congestion is generated at the exit during evacuation. In order to further observe the effect of SD restriction on the generation and dissipation of congestion at the exit, we selected a 10×10 grid

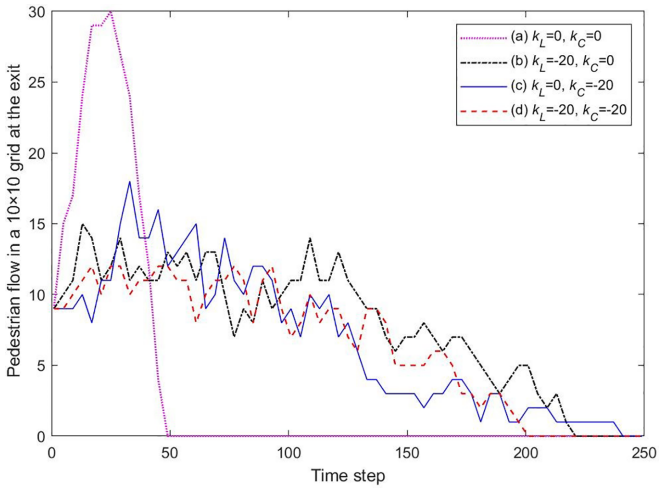

FIG. 3. Number of pedestrians in 10×10 grid at exit changes over time during evacuation.

area at the exit to observe the change of pedestrian flow in this area. Figure 3 shows how the number of pedestrians in this area varies over time during evacuation. It can be seen that the curve trends of combinations (b), (c), and (d) are comparable, with more gradual flow changes than combination (a). Therefore, SD restriction not only reduces close contact between pedestrians but also prolongs the evacuation time of crowds.

In addition, to observe how social groups reshape themselves when attempting to comply with the requirements of physical distancing, we calculated the cumulative SD violations (the events in which the distance between two pedestrians was less than 1 m) in evacuation space and cumulative pedestrian trajectories with the following equations:

$$V_{i,j} = \sum_{t=1}^{t_a} \lambda_{i,j}^{t}, \tag{7}$$

$$T_{i,j} = \sum_{t=1}^{t_a} \mu_{i,j}^{t}, \tag{8}$$

where $V_{i,j}$ represents the number of SD violations occurring at cell (i, j), $T_{i,j}$ represents the number of pedestrian trajectories passing through cell (i, j), t is the tth time step, t_a is the total number of time steps of a simulation, and $\lambda_{i,j}^{t}$ and $\mu_{i,j}^{t}$ both are 0–1 variables that can be defined as follows:

$$\lambda_{i,j}^{t} = \begin{cases} 1, & \text{if the pedestrian at cell } (i, j) \text{ violates the SD restriction at } t \\ 0, & \text{otherwise} \end{cases}, \tag{9}$$

$$\mu_{i,j}^{t} = \begin{cases} 1, & \text{if cell } (i, j) \text{ is occupied by a pedestrian at } t \\ 0, & \text{otherwise} \end{cases}. \tag{10}$$

We drew the heat maps of cumulative SD violations and cumulative pedestrian trajectories for the above four parameter combinations, as seen in Figs. 4 and 5, respectively. Note that the color-bar scale varies for each panel in Figs. 4 and 5. Due to the introduction of the two density fields, the pedestrian dynamics are greatly changed, resulting in significant differences in pedestrian behavior in different parameter combinations. In order to highlight the differences in pedestrian behavior and clearly show the color changes in each panel, different scale ranges are used in the panels of Figs. 4 and 5.

As shown in Fig. 4(a), when moving freely, pedestrians accumulate at exits, resulting in frequent violations of SD. Comparing Fig. 4(b) with Fig. 4(c), we can find that the local density field outperforms the cumulative density field in reducing SD violations. When both are considered [Fig. 4(d)], the close contact of pedestrians at the exit is greatly reduced. In addition, the movement trajectories of pedestrians are analyzed from Figs. 5 and 6 shows the localized enlargement of congestion at the upper exit in each subplot of Fig. 5. When both density fields are not considered, the movement trajectories of pedestrians are more intensive, tending to evacuate along the shortest path directly toward the exit [see Fig. 5(a)]. When the density fields are introduced, the distribution of pedestrian trajectories changes significantly. The local density field makes the trajectory distribution of pedestrians more dispersed [see Fig. 5(b)], while the cumulative density field causes pedestrians to queue up at exits to make room for others [see Figs. 5(c) and 6(c)]. Figure 5(d) shows that the simulation result of introducing both density fields is a superposition of the result of introducing a single density field, with both dispersed trajectory distribution and queuing up at exits.

Through the above visual observations, we know that local density plays a more obvious role in triggering the distance between pedestrians. The effect of cumulative density on SD needs to be further explored.

B. Sensitivity analysis

In order to systematically analyze the variation rule of SD after introducing local density and cumulative density, and to obtain the parameter combination that can maximize the SD between pedestrians, it is necessary to measure the SD violation events. The total number of pedestrians violating the 1-m distance restriction is denoted by VN and their average violating time is denoted by VT. We first ran several pretests by varying the parameter values and found that when $|k_L|$ and $|k_C|$ were greater than 20, VN and VT took values approximately equal to those when $|k_L|$ and $|k_C|$ were 20. VN and VT hardly changed as $|k_L|$ and $|k_C|$ increased, i.e., VN and VT varied only in the range where $|k_L|$ and $|k_C|$ took values from 0 to 20. Thus, the parameters were changed in the range of 0–20, after which VN and VT for different parameter combinations were counted and plotted as heat maps (Fig. 7).

As seen in the left subplot of Fig. 7, VN decreases with the increase of $|k_L|$ and $|k_C|$, indicating that both the local density field and the cumulative density field play a role in limiting the physical distancing between pedestrians. When k_L is fixed and k_C is changed (observe the longitudinal grid color change), the value of VN changes little; when k_C is fixed and k_L is changed (observe the horizontal grid color change), VN greatly decreases with the increase of k_L. Thus, we know that VN is insensitive to the change of cumulative density but sensitive to the change of local density. Using the same method to analyze the right subplot of Fig. 7, it can be seen that VT is more sensitive to cumulative density when k_L is small, whereas the sensitivity of VT to local density does not vary much with $|k_C|$.

To sum up, local density plays a dominant role in limiting proximity, that is, local avoidance of nearby pedestrians can effectively control the distance between pedestrians. Although cumulative density does not directly trigger physical distancing, it can reduce the time pedestrians spend in close contact. When combined, a better SD restriction effect can

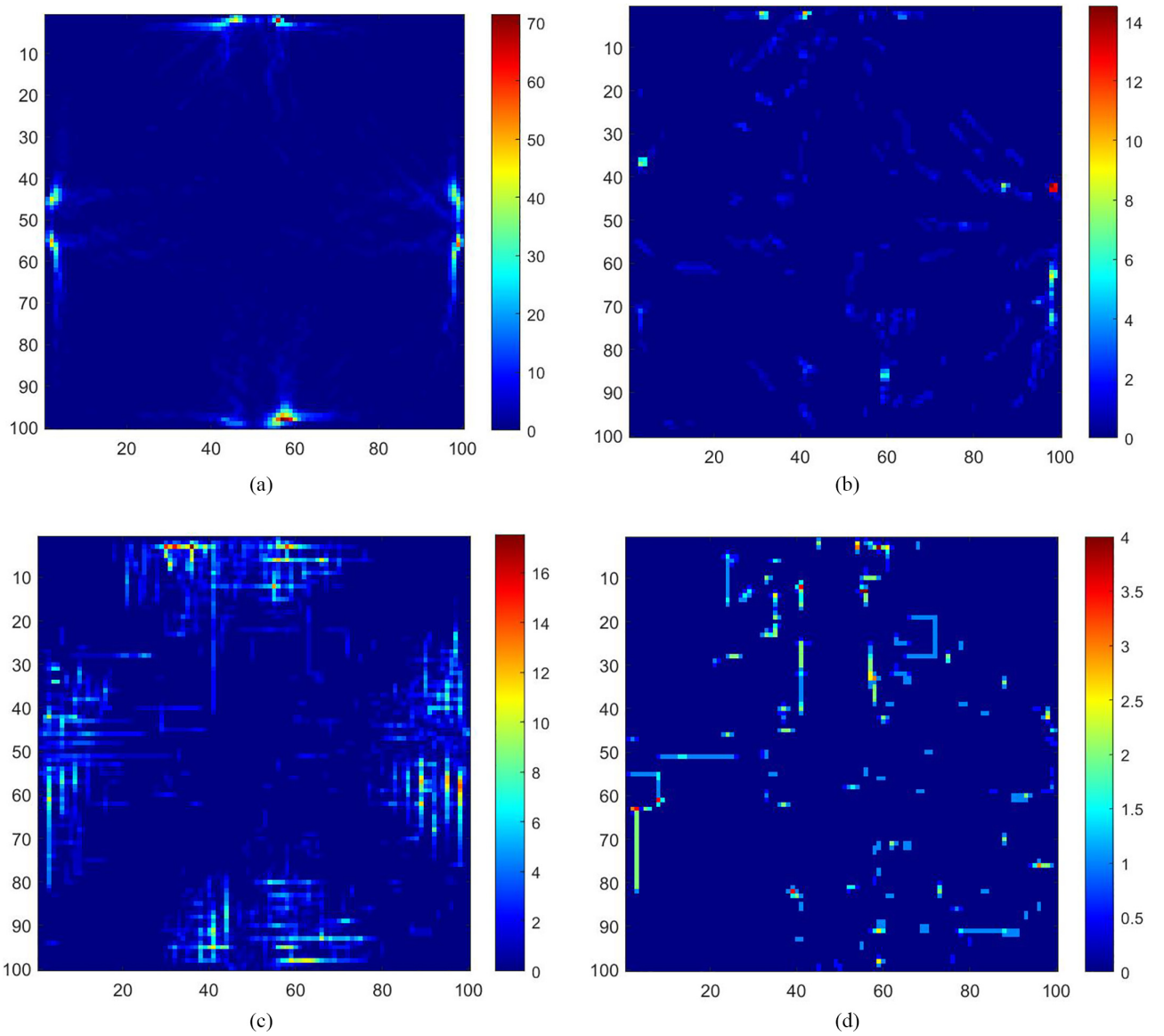

FIG. 4. Heat maps of cumulative SD violations in evacuation space when k_L and k_C take different values: (a) $k_L = 0$, $k_C = 0$; (b) $k_L = -20$, $k_C = 0$; (c) $k_L = 0$, $k_C = -20$; and (d) $k_L = -20$, $k_C = -20$.

be obtained. Moreover, by comparing the total duration of people violating SD, we identify the parameter combination that maximizes SD as $k_L = -18$, $k_C = -19$, which will be applied to the situation of pedestrians complying with SD requirements in subsequent simulation experiments.

IV. MODEL VALIDATION

The fundamental diagram is often used to verify the rationality of pedestrian motion models. Similarly, the model established above can be validated from the perspective of density-velocity relation. As shown in Fig. 8, we perform unidirectional flow simulations in a channel (10 m×3 m) with a periodic boundary. In this scenario, we use the proposed model to carry out two types of pedestrian movement simulation. The first is the normal motion without SD restriction ($k_L = 0$, $k_C = 0$), and is used to compare with the previous unidirectional flow experimental data to prove the reliability of our model. The second is the restricted motion with SD requirement ($k_L = -18$, $k_C = -19$), which is used to explore the impact of SD on the density-velocity relation. We used the classical method to measure the average velocity and density in time and space. First, the 2-m×3-m green rectangle in Fig. 8 is designated as the measurement section. Then, we calculated the ratio of the number of pedestrians to the area of the measurement section as the density, and the mean value of all the pedestrian velocities in the measurement section as the velocity. The equations are as follows:

$$\rho(t)_{\Delta x} = \frac{N(t)}{b_{\mathrm{cor}}\Delta x}, \tag{11}$$

$$v(t)_{\Delta x} = \frac{1}{N(t)}\sum_{i=1}^{N(t)} v_i, \tag{12}$$

where $\rho(t)_{\Delta x}$ represents the density of pedestrians in the measurement area at time t, and $v(t)_{\Delta x}$ represents the average

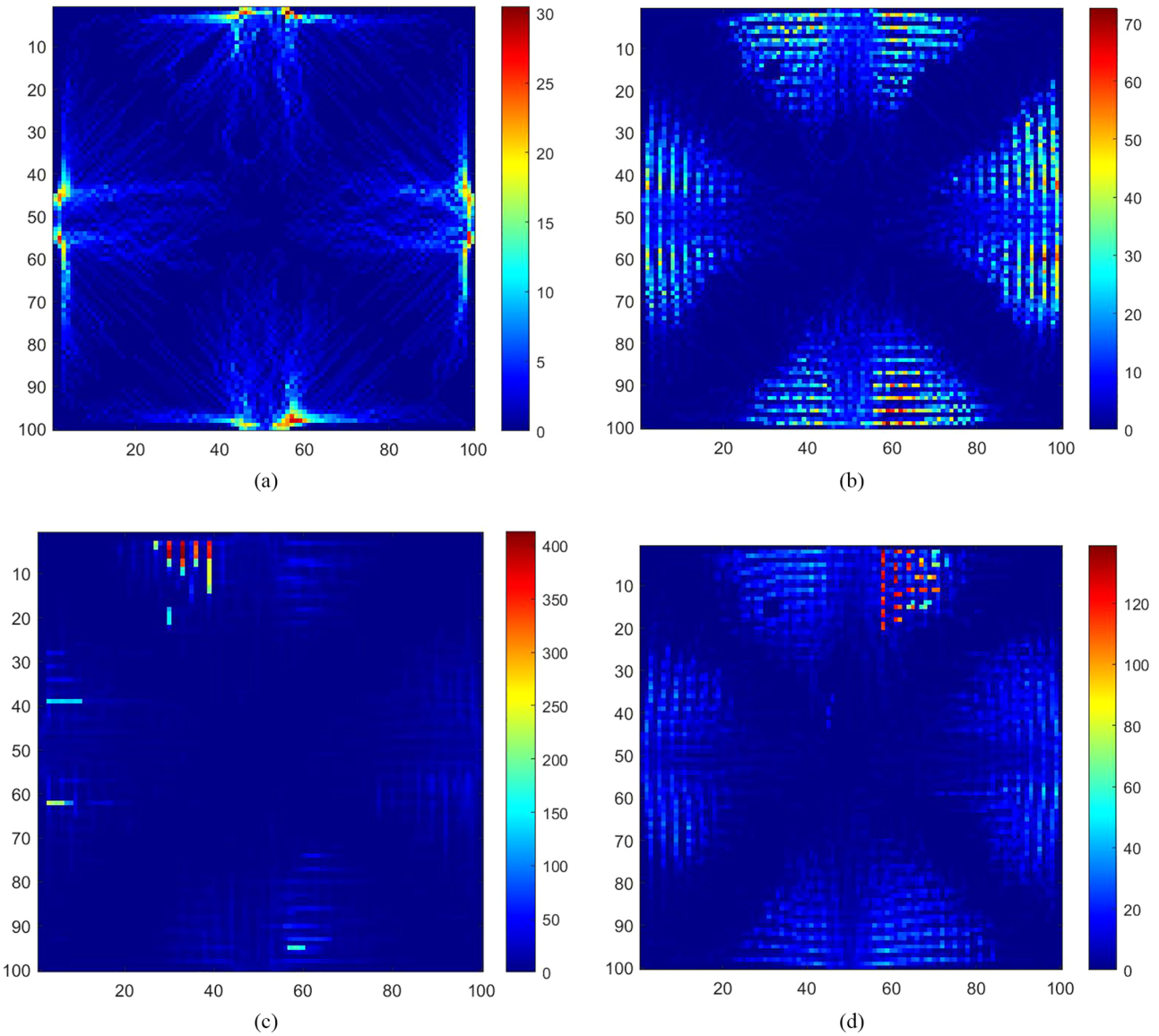

FIG. 5. Heat maps of cumulative pedestrian trajectories in evacuation space when k_L and k_C take different values: (a) $k_L = 0$, $k_C = 0$; (b) $k_L = -20$, $k_C = 0$; (c) $k_L = 0$, $k_C = -20$; and (d) $k_L = -20$, $k_C = -20$.

velocity of all pedestrians in the measurement area at time t; $N(t)$ is the number of pedestrians in the measurement area at time t; b_{cor} is the width of the measurement area; Δx is the length of the measurement area; and v_i is the velocity of pedestrian i in the measurement area, defined as follows:

$$v_i = \frac{\Delta x}{t_{\text{out}} - t_{\text{in}}}, \tag{13}$$

where t_{in} and t_{out} are the moments when pedestrian i enters and leaves the measurement area, respectively.

Identifying the steady state of velocity and density time series, the density-velocity relation can be obtained, as shown in Fig. 9. Through comparison with data obtained from previous unidirectional pedestrian flow experiments [49–52], it can be found that when there is no SD restriction (SD-0; see the red scatters), the density-velocity relation in our study is consistent with the results of real experiments, verifying the rationality of the proposed model. When there is a SD restriction (SD-1; see the green scatters), pedestrians' stopping behavior occurs at a lower density, corresponding to the experimental results of Lu *et al.* [16]. They conducted experiments on pedestrian movement for the SD scenario and the normal scenario, respectively. The experimental results show that in the normal scenario, pedestrians' stopping behavior occurs at a density of $2\,\text{ped}/\text{m}^2$, while pedestrians stop at a density of $1\,\text{ped}/\text{m}^2$ in the SD scenario. The experimental results also provide support for the reliability of our model.

V. MODEL APPLICATION AND ANALYSIS

As seen in the preceding section, SD restriction reduces the proximity of pedestrians and causes pedestrians to congregate longer. Its positive or negative impact on disease transmission is unclear.

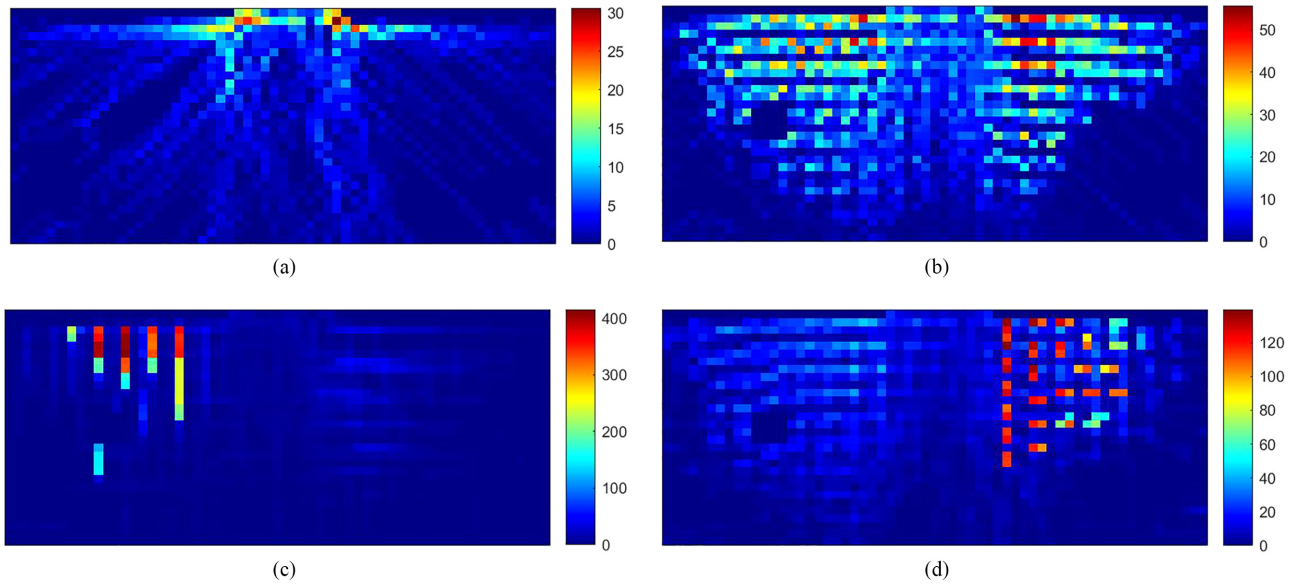

FIG. 6. Enlarged view of congestion at upper exit in Fig. 5.

Transportation hubs, where large numbers of people gather and disperse, often become the source of disease transmission [13]. Therefore, this study selected the waiting hall of a railway station as the research scene to explore how crowd movement affects disease transmission. Figure 10 shows a simplified waiting hall with a grid size of 150×240, including six ticket gates, two exits, and some benches. At the beginning of the simulation, a total of 1500 pedestrians were randomly and evenly distributed in the whole waiting hall space. Suppose that the people in the waiting room immediately initiate an emergency evacuation when they are informed of the presence of patients with a severe infectious disease (the location of the patient is unknown). We compared different scenarios of pedestrian compliance with SD to demonstrate the impact of physical distancing restriction on disease transmission dynamics from various perspectives. The following instructions need to be made before conducting the simulation experiments:

—-Parameter setting of pedestrian movement model:

Pedestrians of SD compliance: $k_S = -5$, $k_O = 2$, $k_L = -18$, $k_C = -19$;
Pedestrians of free movement: $k_S = -5$, $k_O = 2$, $k_L = 0$, $k_C = 0$.

—-Mode of disease transmission:

Since this study was not designed to accurately predict the number of illnesses, the infection assessment module

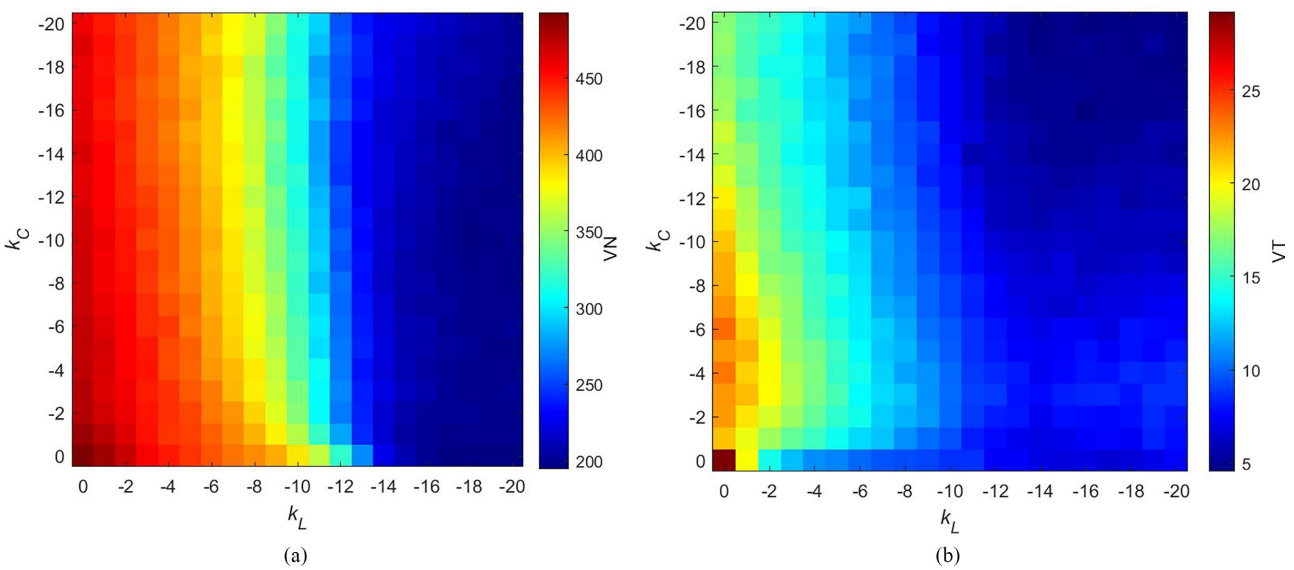

FIG. 7. Heat maps of pedestrian number and duration of SD violation events with different parameter combinations. Left: number of violating pedestrians, VN. Right: average violating time, VT.

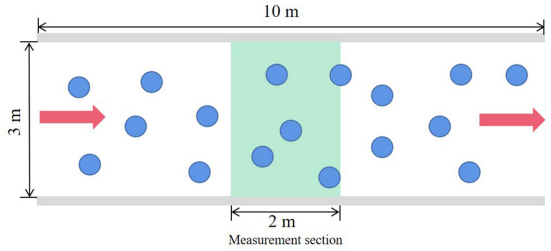

FIG. 8. Sketch of simulation setup, where blue circles represent pedestrians, red arrows represent direction of movement, and 2-m×3-m green rectangle represents measurement section.

developed here is used only to assess the relative risk of disease transmission. Droplets containing the virus are secreted when an infected person coughs or sneezes. These droplets can spread disease if inhaled directly by others. They may also contaminate adjacent surfaces, resulting in subsequent infections among susceptible people. We consider these two modes of infection transmission and define them as person-person transmission and environment-person transmission: (i) Person-person transmission: In our study, when a susceptible person is less than 1 m away from the patient, he will be regarded as a close contact, which is consistent with the World Health Organization's definition [53]. We set the probability of the close contact getting infected as θ_p. (ii) Environment-person transmission: When a patient coughs or sneezes, droplets he secreted spread the virus to surrounding surfaces. We assume that the patient contaminates the cell on which he stands, after which a susceptible person passing through the contaminated cell may become infected with a probability of θ_e.

Many viruses, such as the coronavirus, SARS, influenza, and Ebola, can survive on the surface of inanimate organisms for several days [54]. Compared with the lifespan of these viruses, the duration of our simulation (15 min) is much shorter, so the decay of the virus can be ignored. Before the simulation, the number of infectors is set to ten, and healthy individuals will initially be in a vulnerable state. The

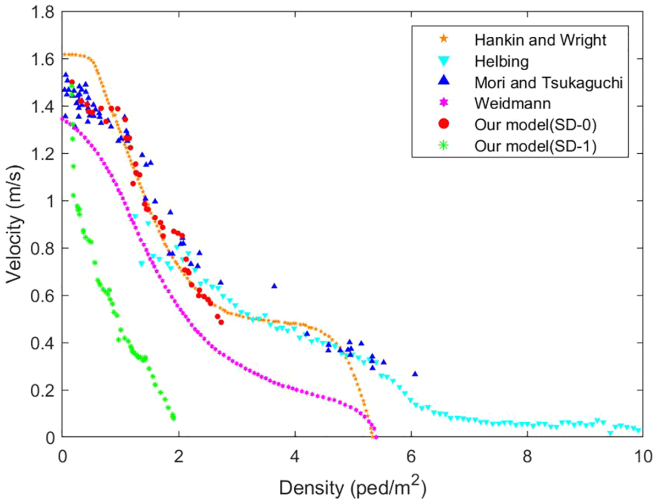

FIG. 9. Fundamental diagrams for unidirectional flow in our model and comparison with experimental data.

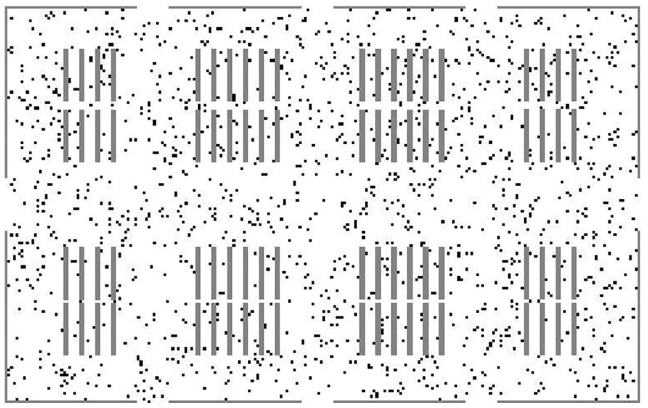

FIG. 10. Simplified waiting hall with 1500 pedestrians randomly distributed. Inside waiting hall, gray dots represent pedestrians, and black bars represent benches; on periphery of waiting hall, there is exit on left and right and three ticket gates on top and bottom.

environment is thought to have been completely sterilized. In this section, the average of the results of 1500 simulation experiments is taken for each case.

A. Influence of social distancing on interpersonal infection and environmental infection

To observe the specific performance of interpersonal infection and environmental infection with the SD restriction, the simulations with different values of θ_p and θ_e were implemented. And, we calculated the difference $\Delta I = I_{\mathrm{SD}-0} - I_{\mathrm{SD}-1}$ in total infections between the no-social distancing scenario (SD-0) and the social distancing scenario (SD-1) when different θ_p and θ_e are combined, as shown in Fig. 11. A greater ΔI means better SD blocking.

As the figure shows, there is a significant difference in the number of infections across the board, confirming the effectiveness of SD. When θ_e is small, ΔI varies greatly with

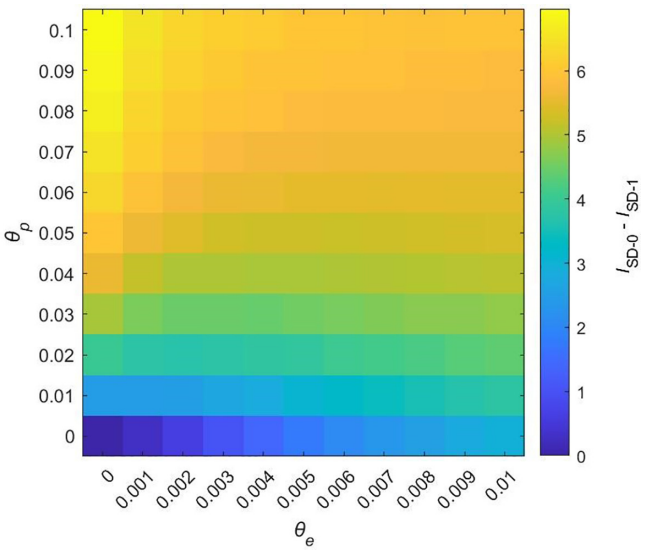

FIG. 11. Difference in total infections between no-social distancing scenario (SD-0) and social distancing scenario (SD-1) with different θ_p and θ_e combinations.

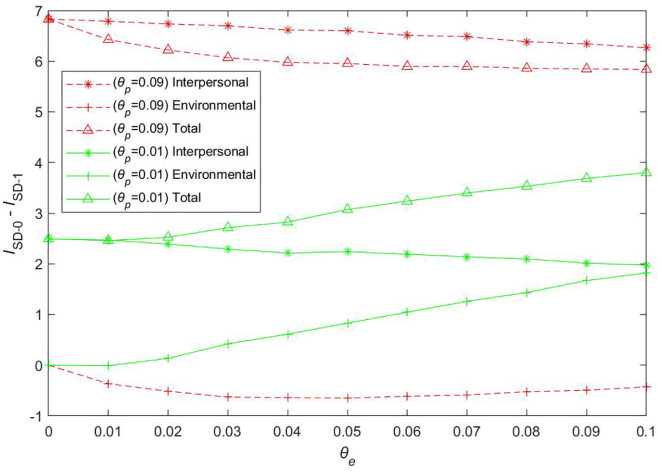

FIG. 12. Curves of ΔI in different infection types for specified θ_p values.

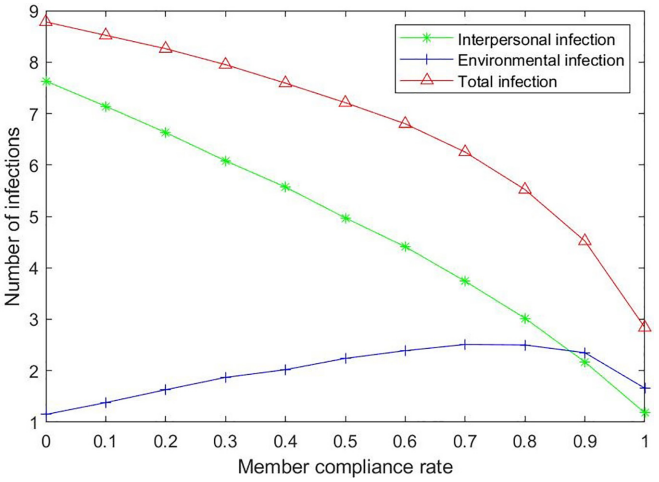

FIG. 13. Number of infections with different member compliance rates.

the increase of θ_p (see the left of Fig. 11). And the larger θ_p and the smaller θ_e, the greater the difference. When θ_p is small, ΔI changes little with the increase of θ_e(see the bottom of Fig. 11). This suggests that interpersonal infection is more sensitive to SD, whereas environmental infection is on the contrary, which is consistent with the former findings [24].

In addition (see the upper part of Fig. 11), when $\theta_p = 0.1$, the value of ΔI gradually decreases as θ_e increases, indicating that environmental infection will offset the effect of SD restriction. This can be explained by the dominance of interpersonal infection and environmental infection in different scenarios. In the SD-1 scenario, person-to-person infections are significantly reduced, while the role of environmental infections is enhanced by an increase in the number of available susceptible people. In other words, even if pedestrians reduce the risk of interpersonal infection by adhering to SD guidelines, they may still inevitably get infected due to environmental transmission. The effectiveness of SD policy depends on interpersonal and environmental transmission probabilities.

To provide a clearer explanation of the intriguing behavior in Fig. 11, where an increase in θ_e leads to an increase in ΔI (total infection) when θ_p is low but results in the opposite trend when θ_p is high, we selected two specific values of θ_p, namely 0.01 and 0.09, and created three corresponding curves of ΔI (interpersonal/environmental/total infection) for each pair of θ values, shown as Fig. 12. It can be seen that when θ_p= 0.09, the total infection ΔI decreases as θ_e increases, which is due to the fact that both interpersonal infection ΔI and environmental infection ΔI decrease. However, when θ_p= 0.01, total infection ΔI increases as θ_e increases, due to the fact that the increase in environmental infection ΔI is greater than the decrease in interpersonal infection ΔI.

B. Influence of social distancing compliance on infection spread

Currently, the field of epidemic-related population psychology offers a wide range of new research methods [30]. For instance, the problem of whether individuals in a crowd comply with SD requirements or engage in risky behaviors in congested scenarios is one of the important elements to explore. It is obvious that the successful implementation of physical distance-related interventions in a crowd depends on the compliance rate of individuals. The number of infections under different member compliance rates is shown in Fig. 13. Here, θ_p is set to 0.1, θ_e is set to 0.01, and the following simulations use the same parameter settings.

It can be seen from Fig. 13 that the total number of infections decreases with increasing member compliance. Compared with the free-flow state, it decreased by about 60% when all members complied with SD restriction, indicating the effectiveness of SD policies in preventing the infection spread. Moreover, SD restriction can help pedestrians avoid physical contact, resulting in an obvious reduction in the number of interpersonal infections.

Moreover, the number of environmental infections increased first and then decreased, which can be explained by the competition between the positive and negative impacts of the SD restriction. On the one hand, crowd evacuation efficiency will be reduced due to the need to maintain physical distance. The more pedestrians adhering to SD requirement, the slower the evacuation, and the longer the susceptible stay in the crowded environment, thus increasing the number of environmental infections. On the other hand, when the crowd moves with the SD restriction, their walking direction is more monotonous and they will not easily change direction (see the red route comparison in Fig. 14), which is consistent with the characteristics of pedestrian movement during the pandemic that we summarized in Sec. II. The monotonous walking direction helps them avoid setting foot in areas contaminated by patients. Therefore, when the SD policy is strictly enforced, it can reduce the risk of environmental infection to some extent.

C. Influence of individual motion heterogeneity on infection spread

To explore the impact of individual SD behavior and group SD behavior on the spread of infection, we set the following four cases of pedestrian movement: (a) The patients comply with SD restriction and the others move freely; (b) The patients move freely and the others comply with SD restriction;

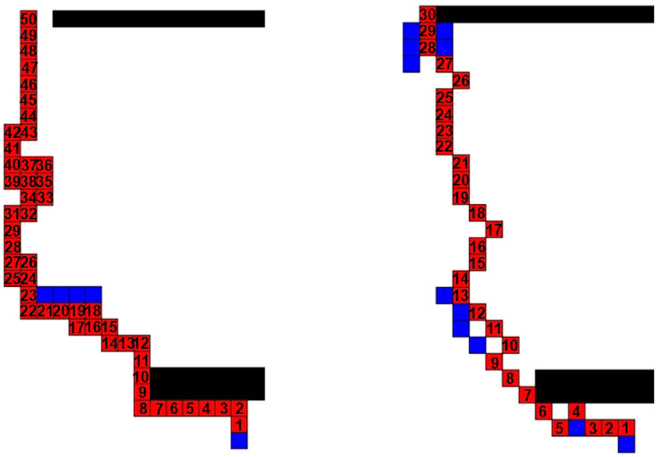

FIG. 14. Movement process of same patient with and without SD restriction, where red represents patient's trajectory, black represents obstacles, blue represents susceptible people in close contact with patient while moving, and number represents sequence of patient's footsteps. Left: with SD restriction. Right: without SD restriction.

(c) All pedestrians comply with SD restriction; and (d) All pedestrians move freely. The infections in the four cases are shown in Table I.

To see this table, the number of total infections is smallest when patients comply with SD restriction and other pedestrians move freely. On the contrary, the infection risk is highest when patients move freely and other pedestrians comply with SD restriction. This is due to the fact that pedestrians other than the patients move with the SD restriction, which slows down the evacuation process and makes them spend more time with the patients; at the same time, the patients' free movement increases their chances of contact with susceptible people, thereby increasing the infection risk. Therefore, it reveals that patients' spontaneous SD behavior and rapid evacuation process play an important role in reducing infection. The trade-off between safety and efficiency associated with SD deserves further exploration.

D. Analysis of crowd evacuation control strategies in the waiting hall

To assess the infection spread dynamics when different evacuation policies are implemented, we calculated the number of infections with different evacuation strategies in both SD-0 and SD-1 scenarios, as shown in Table II. The first strategy is evacuation in batches, which aims to reduce physical contact between people. The second strategy is to add evacuation exits, aiming to enhance evacuation efficiency and thus shorten the time pedestrians spend in dangerous environments. The third strategy is a combination of the first two. We will examine the effectiveness of SD restriction and other control strategies in preventing the spread of disease.

TABLE I. Number of infections in four different pedestrian moving cases.

Case	Number of interpersonal infections	Number of environmental infections	Number of total infections
The patients comply with SD restriction and the others move freely	1.42	0.56	1.98
The patients move freely and the others comply with SD restriction	12.78	3.56	16.34
All pedestrians comply with SD restriction	1.18	1.66	2.84
All pedestrians move freely	7.63	1.15	8.78

It can be seen that in the SD-0 scenario, compared with not taking control measures (8.78), the number of infections could be decreased by using the strategy of evacuation in batches and adding evacuation exits (8.74, 8.41, 8.34, respectively). In the SD-1 scenario, compared with no control measures (2.84), evacuation in batches reduces the evacuation efficiency and increases the infection (3.28), while adding evacuation exits helps rapid evacuation and reduces infection (2.61). Therefore, without compromising the effectiveness of spontaneous SD between pedestrians, managers may need queue management, infrastructure development, and additional resource deployment to speed up pedestrians' movement in the waiting hall.

VI. CONCLUSION

In this work, we considered pedestrian movement characteristics during a pandemic and refined the traditional FFCA model so that SD can be simulated. During the parameter setting, we systematically changed the coefficients of two floor fields related to pedestrian density, which describes the need for pedestrians to avoid crowds. We observed the changing movement behavior of pedestrians with different parameter combinations. Taking 1 m as the threshold of SD, the frequency and duration of SD violations were studied. We examined the influence of different parameters in the movement model on pedestrians' SD behavior and identified the combination of parameters needed to maximize the distance between pedestrians. And, the rationality of our model is verified by the fundamental diagram.

We combined the pedestrian dynamics of physical distancing with the framework of infection spread to evaluate the influence of SD behavior on fine-scale disease propagation. The results reveal that SD policy works well in containing interpersonal transmission, while an increase in environmental transmission can offset some of the effects. The effectiveness of SD depends on interpersonal and environmental transmission probabilities. We also examined the influence of individual motion heterogeneity on infection spread and found that the containment was the best when only patients complied with the SD restriction. Moreover, the trade-off between safety and efficiency associated with SD was also initially explored in this study.

We have tried our best to ensure the validity of our findings, but several limitations remain to be solved in terms of calibrating the parameters and validating our model. First, we did not compare the simulation results with actual data to confirm the accuracy of the proposed model. Second, in the SD-0 version of the model, we have successfully replicated the density-velocity experimental data by only using the static floor field. Thus, exploring which parameters play an important role in determining the shape of the fundamental

TABLE II. Number of infections with different evacuation strategies.

Control strategies		Number of interpersonal infections	Number of environmental infections	Number of total infections
SD-0 scenario	No control measures	7.63	1.15	8.78
	Evacuation in batches	7.52	1.22	8.74 (0.5%↓)
	Adding evacuation exits	7.27	1.14	8.41 (4.2%↓)
	Evacuation in batches + Adding evacuation exits	7.14	1.20	8.34 (5.0%↓)
SD-1 scenario	No control measures	1.18	1.66	2.84
	Evacuation in batches	1.29	1.99	3.28 (15.5%↑)
	Adding evacuation exits	1.12	1.49	2.61 (8.1%↓)
	Evacuation in batches + Adding evacuation exits	1.19	1.83	3.02 (6.3%↑)

diagram is an area that deserves more attention. Third, our assumed probabilities of infection are not purely biological parameters. It is difficult to get the exact values of transmission probabilities by means of experiment, because of the limitations of morality and technology. And, the mechanism of disease transmission in this paper has been simplified. In order to make the simulation of disease transmission more realistic, we can improve the environment-person transmission according to the diffusion process in our future work to simulate the impact of ventilation on disease transmission.

Nonetheless, our work makes a contribution to the growing literature on disease pandemics. This paper emphasizes the need to modify the current tools used in pedestrian dynamic simulation and the necessity of taking the influences of SD on existing pedestrian simulators into consideration. Later researchers can modify our model to allow it to be applicable to the simulation of physical distancing of crowds in more complex spaces. The results of this paper will help policymakers think about different crowd-control strategies to eliminate the potential negative influences of SD requirements on crowd movement as well as on containing the infection spread.

ACKNOWLEDGMENTS

This research was supported by grants from the National Natural Science Foundation of China (Grants No. 72271248, No. 71801227, and No. 72001009), the National Key Research and Development Program of China (Grant No. 2020YFB1600400), the Hunan Provincial Innovation Foundation for Postgraduate (Grant No. 150110081), and the Higher-end Think-Tank Project of Central South University (Grant No. 2022znzk07).

[1] R. J. Littman, Mt. Sinai J. Med. **76**, 456 (2009).
[2] H. Panwar, P. K. Gupta, M. K. Siddiqui, R. Morales-Menendez, P. Bhardwaj, and V. Singh, Chaos Solution Fract. **140**, 110190 (2020).
[3] A. D. Gonçalves, L. H. Fernandes, and A. D. Nascimento, Chaos Solution Fract. **164**, 112634 (2022).
[4] F. Ali, F. Ullah, J. I. Khan, J. Khan, A. W. Sardar, and S. Lee, Chaos Solution Fract. **167**, 112984 (2023).
[5] J. Gross and M. Padilla, From flattening the curve to pandemic: A coronavirus glossary, New York Times (2020), https://www.nytimes.com/2020/03/18/us/coronavirus-terms-glossary.html?searchResultPosition=1.
[6] A. M. Jalali, B. M. Peterson, and T. Galbadage, Front. Public Health **8**, 579559 (2020).
[7] T. Parker-Pope, Deciding how much distance you should keep, New York Times (2020), https://www.nytimes.com/2020/03/19/well/live/coronavirus-quarantine-social-distancing.html?searchResultPosition=2.
[8] R. Foroohar, Covid-19 and the generational divide, Financial Times (2020), https://www.ft.com/content/6a880416-66fa-11ea-800d-da70cff6e4d3.
[9] G. J. Milne, J. K. Kelso, H. A. Kelly, S. T. Huband, and J. McVernon, PLoS One **3**, e4005 (2008).
[10] J. M. Epstein, D. M. Goedecke, F. Yu, R. J. Morris, D. K. Wagener, and G. V. Bobashev, PLoS One **2**, e401 (2007).
[11] J. S. Brownstein, C. J. Wolfe, and K. D. Mandl, PLoS Med. **3**, e401 (2006).
[12] M. T. Vrugt, J. Bickmann, and R. Wittkowski, Nat. Commun. **11**, 5576 (2020).
[13] M. Alam, K. A. Kabir, and J. Tanimoto, J. Stat. Mech. (2020) 033502.
[14] I. Echeverría-Huarte, A. Garcimartín, D. R. Parisi, R. C. Hidalgo, C. Martín-Gómez, and I. Zuriguel, J. Stat. Mech. (2021) 043401.
[15] I. Echeverría-Huarte, R. C. Hidalgo A.Garcimartín, C. Martín-Gómez, and I. Zuriguel, Sci. Rep.-UK **11**, 1 (2021).
[16] T. Lu, Y. Zhao, P. Wu, and P. Zhu, J. Stat. Mech. (2021) 093402.
[17] C. C. Tanis, N. M. Leach, S. J. Geiger, F. H. Nauta, F. Dablander, F. van Harreveld, S. de Wit, G. Kanters, J. Knoppers, D. A. W. Markus *et al.*, Sci. Data **8**, 179 (2021).
[18] S. Hayes, J. Charlton, D. Fletcher, and P. Richmond, Transp. Res. Rec. 1 (2022).
[19] C. A. Pouw, F. Toschi, F. van Schadewijk, and A. Corbetta, PLoS One **15**, e0240963 (2020).
[20] Z. Shao, G. Cheng, J. Ma, Z. Wang, J. Wang, and D. Li, IEEE Trans. Multimedia **24**, 2069 (2021).
[21] M. Rezaei and M. Azarmi, Appl. Sci. **10**, 7514 (2020).
[22] S. Sajjadi, A. Hashemi, and F. Ghanbarnejad, Phys. Rev. E **104**, 014313 (2021).
[23] M. J. Alam, M. A. Habib, and D. Holmes, Transp. Res. Interdiscip. Perspect. **13**, 100527 (2022).

[24] Y. Zhao and R. Geraerts, Automatic parameter tuning via reinforcement learning for crowd simulation with social distancing, in *2022 26th International Conference on Methods and Models in Automation and Robotics* (MMAR) (IEEE, New York, 2022), pp. 87–92.
[25] A. Bouchnita and A. Jebrane, Math. Model. Nat. Phenom. **15**, 31 (2020).
[26] P. C. Silva, P. V. Batista, H. S. Lima, M. A. Alves, F. G. Guimarães, and R. C. Silva, Chaos Solution Fract. **139**, 110088 (2020).
[27] C. M. Mayr and G. Köster, arXiv:2007.01634.
[28] D. R. Parisi, G. A. Patterson, L. Pagni, A. Osimani, T. Bacigalupo, J. Godfrid, F. M. Bergagna, M. R. Brizi, P. Momesso, F. L. Gomez *et al.*, arXiv:2009.04019.
[29] M. Haghani, Safety Sci. **153**, 105818 (2022).
[30] H. Cui, J. Xie, M. Zhu, X. Tian, and C. Wan, Phys. A **608**, 128284 (2022).
[31] Z. Fang, Z. Huang, X. Li, J. Zhang, W. Lv, L. Zhuang, X. Xu, and N. Huang, arXiv:2002.10616.
[32] C. Z. Xie, T. Q. Tang, P. C. Hu, and H. J. Huang, J. Transp. Saf. Secur. **14**, 1063 (2022).
[33] P. Derjany and S. Namilae, Computational model for pedestrian movement and infectious diseases spread during air travel, in *2018 AIAA Modeling and Simulation Technologies Conference* (AIAA, Reston, 2018), p. 0419.
[34] S. Namilae, P. Derjany, A. Mubayi, M. Scotch, and A. Srinivasan, Phys. Rev. E **95**, 052320 (2017).
[35] C. Y. Li and J. Yin, Transportmetrica A **19**, 2005182 (2023).
[36] T. Harweg, D. Bachmann, and F. Weichert, J. Public Health **31**, 221 (2023).
[37] T. Dbouk and D. Drikakis, Phys. Fluids **32**, 053310 (2020).
[38] K. Yamaguchi, Y. Takebayashi, M. Miyamae, A. Komazawa, C. Yokoyama, and M. Ito, Psychol Trauma **12**, S49 (2020).
[39] R. W. Rogers, J. Psychol. **91**, 93 (1975).
[40] P. D. Lunn, S. Timmons, C. A. Belton, M. Barjaková, H. Julienne, and C. Lavin, Soc. Sci. Med. **265**, 113478 (2020).
[41] N. Legate, T. V. Ngyuen, N. Weinstein, A. Moller, L. Legault, Z. Vally, and C. E. Ogbonnaya, Proc. Natl. Acad. Sc. **119**, e2111091119 (2022).
[42] A. R. Ahmad and H. R. Murad, J. Med. Internet. Res. **22**, e19556 (2020).
[43] A. Schadschneider, A. Kirchner, and K. Nishinari, CA approach to collective phenomena in pedestrian dynamics, in International Conference on Cellular Automata (Springer, Berlin, 2002), pp. 239–248.
[44] S. Bandini, M. Mondini, and G. Vizzari, Transp. Res. Part C-Emerg. Technol. **40**, 251 (2014).
[45] P. Degond, C. Appert-Rolland, M. Moussaid, J. Pettré, and G. Theraulaz, J. Stat. Phys. **152**, 1033 (2013).
[46] E. Dudek-Dyduch and J. Wąs, Knowledge representation of pedestrian dynamics in crowd: Formalism of cellular automata, in *Artificial Intelligence and Soft Computing–ICAISC 2006: 8th International Conference* (Springer, Berlin, 2006), pp. 1101–1110.
[47] P. Zhang, X. X. Jian, S. C. Wong, and K. Choi, Phys. Rev. E **85**, 021119 (2012).
[48] H. Zhao, J. Comput. Math. **25**, 421 (2007).
[49] B. D. Hankin and R. A. Wright, J. Oper. Res. Soc. **9**, 81 (1958).
[50] M. Mori and H. Tsukaguchi, Transport. Res. A-General **21**, 223 (1987).
[51] U. Weidmann, Schriftenreihe Des IVT **90**, 1 (1992).
[52] D. Helbing, A. Johansson, and H. Z. Al-Abideen, Phys. Rev. E **75**, 046109 (2007).
[53] World Health Organization, Coronavirus disease 2019 (COVID-19): Situation report 75 (2020), https://apps.who.int/iris/handle/10665/331688.
[54] S. Yang, Y. Wu, Y. Qu, Q. Liu, H. Wu, Y. Gong, and J. Ma, Res. Environ. Sci. **33**, 1617 (2020).